Journal of Materials Chemistry A

RSC Publishing

PAPER

View Article Online
View Journal | View Issue

Cite this: J. Mater. Chem. A, 2013, 1, 15479

Photocurrent improvement in nanocrystalline Cu_2ZnSnS_4 photocathodes by introducing porous structures†

Xin Wen, Wenjun Luo* and Zhigang Zou*

Received 11th October 2013
Accepted 23rd October 2013

DOI: 10.1039/c3ta14096b

www.rsc.org/MaterialsA

Cu_2ZnSnS_4 (CZTS) is a potential low-cost photocathode material for solar water splitting. In this study, we prepare dense and porous nanocrystalline Cu_2ZnSnS_4 films by a facile metal organic decomposition (MOD) method. The porous structures are adjusted by varying the amount of thiourea in the precursor solution. The porous CZTS photocathode yields 3 times higher photocurrent than that of the dense electrode. Thermogravimetric/differential thermal analysis shows that the porous structure comes from decomposition of excess thiourea. Different characterization methods, such as X-ray diffraction, Raman spectroscopy, energy-dispersive X-ray spectroscopy, SEM and UV-vis-NIR transmission, have been carried out to analyze the mechanism of photocurrent improvement. The results suggest that the dense and the porous CZTS photocathodes have similar crystallinity, composition, thickness and light absorption. The relative electrochemical active area indicates that shortening of the electron transport distance is a possible reason for photocurrent improvement in the porous CZTS photocathode.

1. Introduction

Solar water splitting for hydrogen production is a promising approach to solar energy conversion and storage. Since the pioneering work of Fujishima and Honda,[1] photoelectrochemical water splitting has been intensively studied by different researchers in the past forty years.[2,3] Some visible-light-response and efficient photoanodes for water oxidation, such as WO_3, Fe_2O_3, $BiVO_4$ and Ta_3N_5, have been investigated by us and other authors.[4–9] However, one of the key challenges for these photoanodes is that an external bias should be offered to split water due to a low conduction band bottom or a high overpotential. A Si based or dye-sensitized solar cell is usually used to offer the bias.[5] However, the additional cell makes the photoelectrochemcial water splitting cell more complicated and expensive. The use of a simple p–n two photon PEC cell is a very promising method to solve the problem.[2,10] In the p–n cell, an n type photoanode for water oxidation is connected with a p type photocathode for proton reduction in series. In order to split water without a bias, the valence band top of the photoanode is lower than the water oxidation potential and the conduction band bottom of the p type is higher than proton reduction potential. Moreover, the conduction band bottom of the photoanode is higher than the valence band top of the photocathode. Therefore, a low cost and band match p type photocathode is highly desired to be assembled with the photoanode to realize solar water splitting under zero bias.

Though some p type photocathodes, such as Si, InP, GaAs and Cu(In,Ga)Se_2 (CIGS), have been studied intensively,[11–14] the mismatched band positions of Si or the scarcity of In or Ga in the earth limit their practical applications. Recently, a p type material Cu_2ZnSnS_4 (CZTS), as a light absorption material in a solar cell, has attracted wide interest due to its suitable band gap (about 1.5 eV), high absorption coefficient (10^4 cm^{-1}), abundance and non-toxicity. The band positions of a CZTS photocathode can match with the above mentioned $BiVO_4$ or Ta_3N_5 photoanodes very well in our previous study.[15] In theory, they can be assembled into a p–n cell and realize solar water splitting without an external bias. Compared with CZTS as a solar cell material,[16–18] research on CZTS as photocathodes for water splitting is limited.[15,19–21] In a solar cell, a dense film is necessary because the photo-generated carriers should diffuse long distance to the junction region, where the photo-generated carriers are separated. Therefore, a high crystalline sample in a solar cell often indicates higher performance than a poor crystalline one. However, in a photoelectrochemical water splitting cell, a Schottky junction forms at the solid–electrolyte interface and separates photo-generated carriers. A porous thin film can obtain higher performance than a dense sample due to stronger light absorption and/or shorter transport distance of photo-generated carriers.[22–28] Therefore, it is possible to obtain a high efficiency cell in poor crystalline samples, which can lower the fabrication cost of a photoelectrochemical cell.

Ecomaterials and Renewable Energy Research Center, National Laboratory of Solid State Microstructures, Department of Physics, Nanjing University, Nanjing, 210093, China. E-mail: wjluo@nju.edu.cn; zgzou@nju.edu.cn

† Electronic supplementary information (ESI) available. See DOI: 10.1039/c3ta14096b

In this work, we employed a facile method to control the porous structures of the CZTS thin films and investigated the effect of the porous structure on the photoelectrochemical properties. The CZTS samples were prepared by a metal organic decomposition (MOD) method. Thiourea was used as a sulfur source, stabilizer and pore-forming agent. By adjusting the amount of thiourea, the dense and the porous CZTS thin films were obtained. The photocurrent of the porous CZTS photocathode was much higher than that of the dense sample. Further analysis suggested that the photocurrent enhancement came from the decrease of minority carrier transport distance, not from stronger light absorption. In previous studies, different porous CZTS samples have been studied as counter electrodes in DSSCs or lithium batteries,[29,30] however, there are few reports on the porous CZTS in a photoelectrochemical water splitting cell.

2. Experimental section

2.1 Preparation of the CZTS thin films

The precursor solutions were prepared by dissolving copper(II) acetate monohydrate (0.14 mol L^{-1}), tin(II) chloride dihydrate (0.11 mol L^{-1}), zinc chloride (0.1 mol L^{-1}), and thiourea (0.5 or 1 mol L^{-1}) in methanol with optimized ratios of Cu : Zn : Sn : S = 1.4 : 1 : 1.1 : 5 and 1.4 : 1 : 1.1 : 10 for the dense and the porous samples, respectively. The solutions were transparent and colorless. The FTO substrates were cleaned by ultrasonication in HCl and washed with acetone and deionized water. The precursor solution was spin-coated onto the FTO substrate at 1500 rpm for 1 min followed by heating at 580 °C in N_2 for 2.5 min. The coating step was repeated six or four times for the dense or the porous samples, respectively, to obtain CZTS films with a similar thickness.

2.2 Characterization of the samples

The crystal structures of the films were measured by X-ray diffraction (XRD, Rigaku, Ultima III). The Raman spectra were recorded using a Visible and UV Laser Raman spectrophotometer (JY-HR800) for excitation wavelength at 488 nm and 325 nm. The Raman spectra were calibrated by Si (520 cm^{-1}). The morphologies and elemental ratios of the samples were examined with a scanning electron microscope (SEM, EDX, Nova NanoSEM 230 FEI Co). In order to avoid the influence of SnO_2, XRD and EDX data were obtained with the samples prepared on glass substrates not FTO glass substrates. The transmission spectra of the films were recorded with a UV-visible-NIR spectrophotometer (UV-3600, Shimadzu). The thermogravimetric/differential thermal analysis (TG/DTA) was performed using a thermoanalytical apparatus (STA 449 C, NETZSCH) under a N_2 atmosphere at a heating rate of 10 °C min^{-1}.

2.3 Photoelectrochemical and electrochemical characterization

The photoelectrochemical properties of the CZTS photocathodes were measured in a conventional three-electrode cell using an electrochemical analyzer (CHI-633C, Shanghai Chenhua, China). The prepared CZTS photocathode was used as the working electrode and a Pt foil and a saturated calomel electrode (SCE) as the counter electrode and the reference electrode, respectively. An aqueous solution containing 0.5 M Na_2SO_4 (pH = 6) was used as the electrolyte and the light source was a Xe lamp. Before measurement, N_2 was bubbled into the electrolyte for half an hour to remove oxygen in the electrolyte. The samples were illuminated from the front side (electrolyte–semiconductor interface) and cycling voltammetry measurements were scanned at a speed of 10 mV s^{-1}. Potentials of the working electrode were given in a RHE scale to easily compare with other results by the formula $V_{RHE} = V_{SCE} + 0.242V + 0.059 \times$ pH, where V_{RHE} was the potential *vs.* a reversible hydrogen potential, V_{SCE} was the potential *vs.* SCE electrode, and pH was the pH value of the electrolyte. The incident photon-to-current efficiency (IPCE) was determined under illumination of different wavelength light generated by monochromatic filters. The IPCE was calculated as follow:

$$\mathrm{IPCE} = \frac{1240 \times I_{ph}}{p \times \lambda}$$

where I_{ph} is the photocurrent density (μA cm^{-2}), P and λ are the incident light intensity (μW cm^{-2}) and wavelength (nm), respectively. The incident light intensity was measured using a photometer (Newport, 840 C, USA). Faradaic efficiency was measured at −0.2 V_{RHE} in 0.5 M Na_2SO_4 (pH = 6) aqueous solution under full arc Xe lamp illumination. The area of the sample was about 2 cm^2. The three-electrode cell was sealed and was purged by Ar for half an hour and no O_2 or N_2 was detected before the Faradaic efficiency measurement. Evolved H_2 and O_2 gases were detected using an on-line gas chromatograph (Agilent, 490 Micro GC). The relative electrochemical surface area was determined by capacitive current between 0.5 V_{RHE} and 0.7 V_{RHE} in 0.5 M Na_2SO_4 aqueous solution in the dark. The scan rate was changed from 25 to 300 mV s^{-1}.[31]

3. Results and discussion

3.1 Formation mechanism of the porous structure

The surface and cross-sectional SEM images of the CZTS films are shown in Fig. 1. The sample with thiourea/zinc = 5 consists of densely packed nanocrystallites, while obvious porous structures are observed in the sample with thiourea/zinc = 10. They are named as dense and porous samples in this study, respectively. The shapes of pores are irregular and their sizes range from 50 nm to 300 nm in the porous sample. The thicknesses of the two samples are similar and about 500 nm. More pores are observed on the surface than on the cross-section (see Fig. 1(b) and (d)). It is because that the precursor solution was repeatedly spin-coated onto substrates followed by heat treatment, the pores in the first layer can be filled with nanocrystals synthesized in the second layer. Porous structures are also observed in the samples with thiourea/zinc = 7.5 and 12.5 (Fig. S1†). Here, the samples with thiourea/zinc = 5 and 10 as representatives are discussed in detail.

In order to investigate the formation mechanism of the pore structure, the thermogravimetric/differential thermal analysis

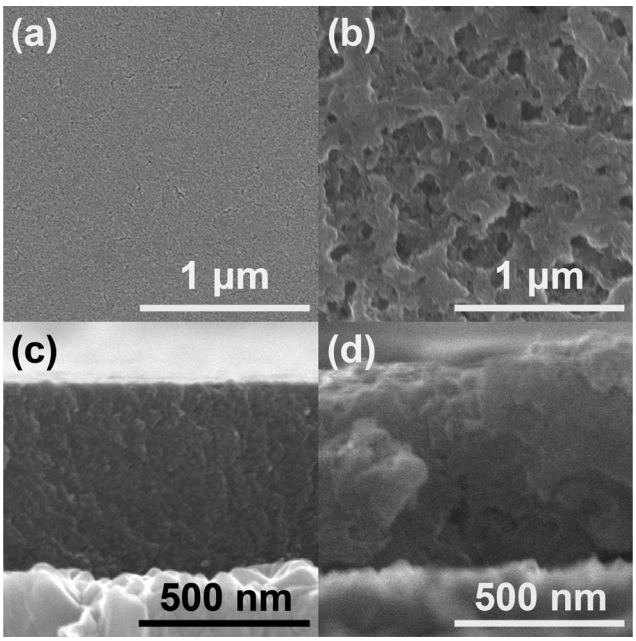

Fig. 1 Surface and cross-sectional SEM images of the CZTS films prepared with the precursor solution of thiourea/zinc ratios 5 (a and c) and 10 (b and d).

(TG/DTA) was carried out and the results are shown in Fig. 2. In the range of room temperature to 180 °C, endothermic peaks are observed. According to the literature,[32] these peaks can be assigned as follows. The peak shoulder from 50 °C to 75 °C can be attributed to the evaporation of the remaining solvent. The peak at 96 °C is due to dehydration of crystal water in precursor copper acetate and tin chloride. The peak at 148 °C is related to the melting of precursor compounds. The huge mass loss over the temperature range 200–300 °C is caused by decomposition of excess thiourea, which starts to decompose at 200 °C and the byproduct NH_4Cl decomposes at 310 °C.[30] Therefore, the pore formation comes from decomposition of the excess thiourea. To further verify the formation mechanism of the pore structures, we investigated the morphologies of the films prepared at different temperatures (200 °C, 250 °C and 300 °C) for the same

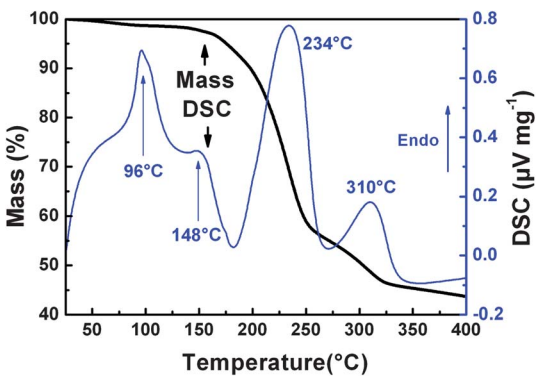

Fig. 2 Thermogravimetric/differential thermal analysis (TG/DTA) of the precursor solutions with thiourea/zinc = 10 after being dried at 60 °C in air. TG/DTA was conducted in a N_2 atmosphere with a temperature increasing rate of 10 °C min^{-1}.

time. The film with the thiourea/zinc = 10 solution shows dense morphologies at 200 °C but porous at 250 °C and 300 °C, while the film with the thiourea/zinc = 5 solution at 200–300 °C always shows dense morphologies (Fig. 3). Therefore, thiourea plays an important role as a pore-maker besides as a sulfur source and a stabilizer.

The pore formation mechanism is similar to the results reported by Yin *et al.*[30] However, obvious different morphologies are obtained in the present study. The pore size here is much smaller than that by Yin's method. Moreover, the film prepared in this study shows a flatter surface than that by Yin's method. This difference could be attributed to the different precursor solutions and different preparation processes. The aqueous solution and drop-coating were used in Yin's study, while the methanol solution and a high-speed spin-coating were used in this report. In Yin's drop pyrolysis method, a relatively large amount of precursor solution was dropped onto the substrate at 150 °C and fast evaporation of water and pyrolysis of precursors occurred. It is noted that not only the decomposition of excess thiourea contributed to their porous structure but also the fast evaporation of water in Yin's method. In this report, only a thin layer of precursor solution covered the substrate after a spin-coating process and a small amount of methanol remained on the film before heating and decomposition of the excess thiourea, which made the pore size smaller and the film flatter. The uniformity of the thickness in Yin's method is very poor and is not suitable for photoelectrochemical applications because the photoelectrochemical property of a film depends on the thickness very sensitively. Therefore, these flatter samples indicate more advantages than Yin's when they are used as photoelectrodes.[33,34]

3.2 Composition of the dense and the porous samples

In order to identify the phases of the two samples, X-ray diffraction patterns were measured and the results are shown in Fig. 4. The peaks at $2\theta = 28.3°$, 47.3° and 56.2° are assigned to diffraction of the (112), (220) and (312) planes of Kesterite CZTS (PDF cards 00-026-0575).[35] According to the Scherrer equation, the crystal sizes of the dense and the porous samples are 18.3 nm and 24.3 nm, respectively. The results are reasonable since our samples were only calcined for a very short time. The broad peaks also show characteristics of the nanocrystalline photoelectrode. Compared with a microcrystalline sample, a nanocrystalline photoelectrode has a shorter transport distance to the interface and reduces the recombination possibility of photo-generated carriers. Therefore, a nanocrystalline photoelectrode is often used to improve solar conversion efficiency of a photoelectrochemical cell.[36,37]

XRD cannot distinguish other impurities, such as ZnS and Cu_2SnS_3 from CZTS due to very similar XRD patterns.[35] Therefore, Raman spectroscopy was employed to investigate other impurity phases and the results are indicated in Fig. 5(a). Both the Raman spectra show a similar peak at 338 cm^{-1} with a shoulder of 287 cm^{-1}, which is assigned to CZTS.[38] No Cu_2SnS_3 peaks at 303 cm^{-1} are observed. Moreover, visible Raman spectra at 488 nm have a very weak signal on a ZnS sample

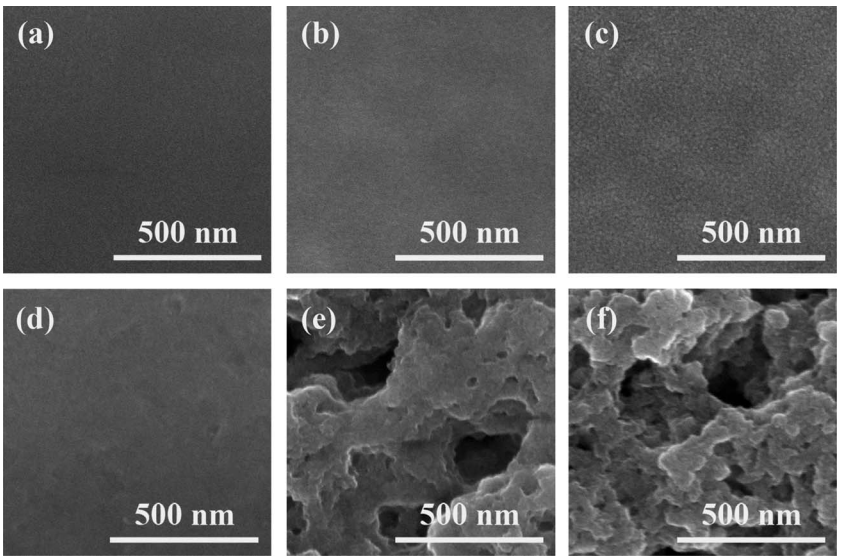

Fig. 3 SEM images of the samples prepared with the precursor solutions of thiourea/zinc = 5 at 200 °C (a), 250 °C (b), 300 °C (c) and thiourea/zinc = 10 at 200 °C (d), 250 °C (e), 300 °C (f) for 20 min, respectively.

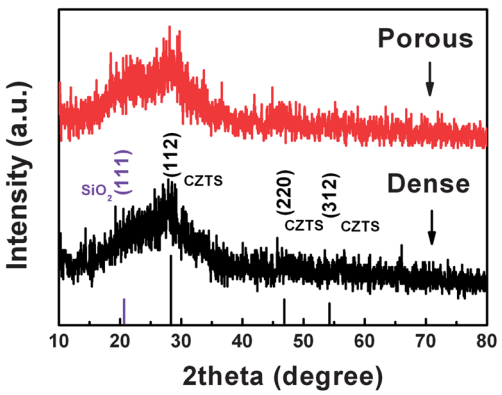

Fig. 4 XRD pattern of the dense and the porous CZTS samples.

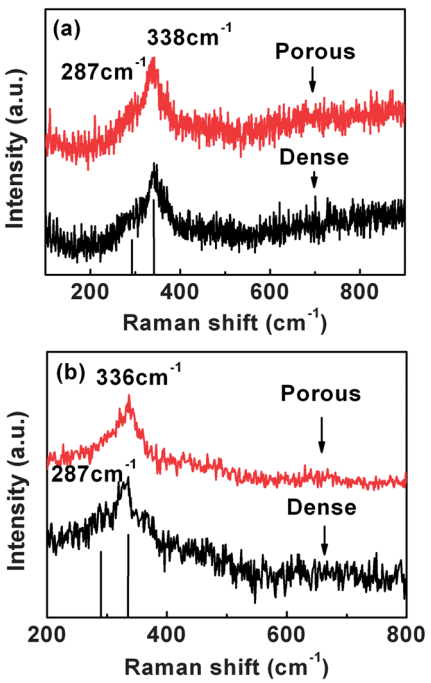

Fig. 5 Raman spectra of the dense and the porous CZTS films excited by a laser with the wavelength of 488 nm (a) and 325 nm (b), respectively.

under nonresonant excitation conditions and are not suitable to detect the ZnS impurity phase.[39] Therefore, we recorded ultraviolet Raman spectra with an excitation wavelength at 325 nm to detect ZnS. Only a mode at 337 cm^{-1}, no ZnS Raman peaks at 350 cm^{-1} and 700 cm^{-1} are observed. A post-annealing procedure (sulfurization) is generally employed to increase the crystallinity of CZTS.[40] However, in this report, the nanocrystalline CZTS samples have not been subjected to sulfurization, which results in poor crystallinity. A small amount of ZnS and/or Cu_2SnS_3 impurities could not be excluded from the samples due to the weak XRD and Raman signals of the nanocrystalline. CZTS is the main phase in our samples.

Since the elemental ratios of the samples have an important effect on photoelectrochemical performance, we also measured the elemental ratios by EDX and the results are shown in Table 1. Both the samples exhibit Cu-poor and zinc-rich characteristics, which is a typical feature of a high efficiency CZTS solar cell. The record conversion efficiency of the CZTS solar cell has ratios of Cu/(Zn + Sn) and Zn/Sn of about 0.8 and 1.2, respectively.[18] In our experiments, the optimized ratios of Cu/(Zn + Sn) and Zn/Sn are 0.65 and 1.27, respectively. The theoretical calculation suggests that the dominant acceptor defect will change with composition.[41,42] The Cu_{Zn} antisite energy level is

Table 1 Elemental ratios of the dense and the porous CZTS films by EDX

	Dense	Porous
Zn/Sn	1.20	1.27
Cu/(Zn + Sn)	0.64	0.65
S/Metal	0.75	0.73

the lowest acceptor defect energy level in stoichiometric CZTS and it is about 0.12 eV above the valence band maximum. However, the feature of Cu-poor and zinc-rich in CZTS possibly changes the lowest acceptor defect energy level with Cu^+ vacancy defects, which is about 0.02 eV above the valence band maximum. The decrease of the dominant acceptor defect energy level can increase the density of majority carriers and enhance the efficiency of CZTS. Sulfur deficient characteristic of our samples is observed, which is related to the rapid decomposition of thiourea under high temperature.

3.3 Effect of the porous structure on the PEC performance

Fig. 6(a) shows the PEC performance of the two CZTS samples in 0.5 M Na_2SO_4 under Xe lamp illumination. The cathodic photocurrent is observed in the two samples, which indicates that the CZTS samples are p-type semiconductors. The porous film has 3 times higher photocurrent at -0.4 V_{RHE} than the dense film. In order to confirm that the improved photocurrent is not caused by the capacity effect, a current–time curve at a constant potential (the inset of Fig. 6(a)) is also measured. The same conclusions are obtained, which excludes the effect of the capacitive current. Moreover, the porous film shows much higher transient photocurrent spikes than the dense film. The transient current spikes come from the accumulation of photogenerated carriers at the semiconductor–liquid interface. The absence of transient photocurrent spikes of the dense sample suggests that the carrier transport processes in the dense film are limited by recombination in the bulk, not the surface.[36] Fig. 6(b) shows the IPCE of the two CZTS samples. The porous sample achieves an IPCE of 4.5% at 0 V_{RHE}, which is about 2.5 times as high as that of the dense sample. The results are consistent with the photocurrent. The photoelectrochemical performance of the CZTS samples with other ratios of thiourea/zinc = 7.5 and 12.5 was measured and the results are shown in Fig. S2.† The photocurrents of the samples with ratios of thiourea/zinc of 7.5, 10 and 12.5 are all higher than that of the dense sample with a ratio of 5.

Moreover, the stability and Faradaic efficiency of a photoelectrode are important. A longer duration stability test of the CZTS sample was carried out and the results are shown in Fig. S3.† The stability of a bare CZTS photocathode is poor and can be improved by loading Pt on the surface. The Pt loaded porous CZTS sample also shows higher photocurrent than that of the Pt loaded dense sample (Fig. S4†). Therefore, it is concluded that the porous sample has a better photoelectrochemical performance than the dense sample, no matter with Pt loading or not. Even though, the stability of the Pt loaded CZTS photocathode is still poor, the results are similar to a recent literature.[21] Stability can be further improved by depositing protective layers.[19,21] We are trying to do that. To investigate the origin of the photocurrent, Faradaic efficiencies of H_2 and O_2 need to be measured. Because of the poor stability of a bare CZTS photocathode as mentioned above, it is difficult to measure Faradaic efficiencies of H_2 and O_2 on a bare CZTS photocathode. Pt loading can improve the stability of the CZTS photocathode for water reduction. Therefore, we measured Faradaic efficiencies (Fig. S5†) of H_2 and O_2 on the Pt loaded porous sample, which are 84.3% and 81.3%, respectively. The results suggest that the photocurrent mainly comes from water splitting reaction, not film self-corrosion.

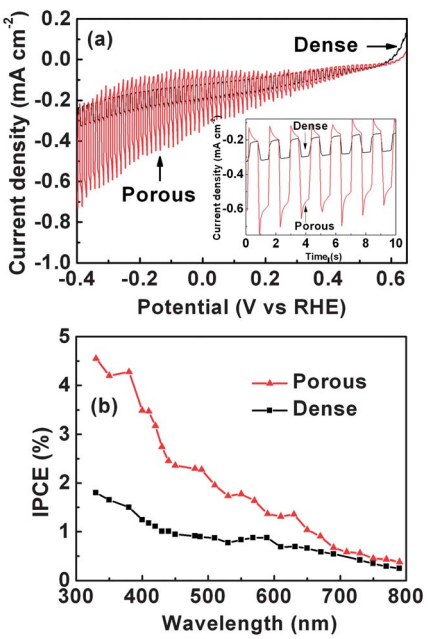

Fig. 6 (a) Photocurrents *vs.* potential curves of the dense and the porous CZTS photocathodes in 0.5 M Na_2SO_4 (pH = 6) aqueous solutions under 500 W full arc Xe lamp illumination. The inset shows *i–t* curves measured at a constant potential of -0.4 V_{RHE}. (b) IPCE of the dense and the porous samples at 0 V_{RHE} in 0.5 M Na_2SO_4 (pH = 6) aqueous solution.

3.4 A mechanism of photocurrent improvement in the porous photoelectrode

Since the crystallinity, bulk composition and thickness of the dense and the porous samples are similar by the above analysis, two other reasons are possibly responsible for the improved photocurrent in the porous photoelectrode. One is stronger light absorption and the other is a shorter transport distance of minority carriers.[22–28] Incident light is scattered by the pores in the film thus increasing the possibility of being absorbed. This effect has been utilized to improve the photoelectrochemical or photocatalytic performance of other materials.[22–24] The UV-vis-NIR transmission spectra of the two samples were recorded to identify the pores effect on the optical absorption. Fig. 7 shows the UV-vis-NIR transmission spectra of the dense and the porous CZTS films. The band gaps of the two samples are both estimated to be 1.53 eV from the inset of Fig. 7, which further confirms that the CZTS samples are pure phases. The transmission of the porous film is slightly lower than that of the dense sample, which suggests that the pores do not enhance optical absorption. This result is different from the literature because the porosity of the CZTS film is not high enough (see Fig. 1). Seel *et al.* investigated the absorption of a porous Si thin film by both the analytical model and experiment, and they found that the porous Si thin film with a porosity of 30% had

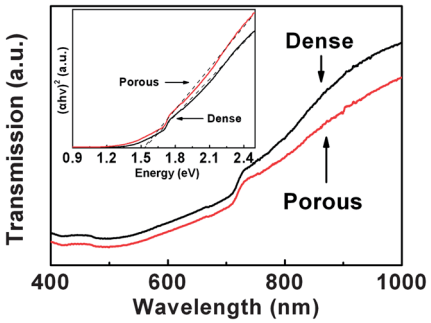

Fig. 7 UV-vis-NIR transmission spectra of the dense and the porous CZTS films.

enhanced light absorption as the pore size increased due to enhanced light scattering in the material.[23] The porous CZTS sample has 3 times higher photocurrent than that of the dense sample, however, their optical absorption is close. Therefore, the optical absorption enhancement in the porous sample does not play a major role in photocurrent improvement.

Since stronger light absorption is not the main reason for photocurrent improvement in the porous electrode, the other effect of the porous electrode, shorter carrier transport distance, was investigated. The relative electrochemical area was measured following Jaramillo's method to understand this effect (see Fig. 8).[31] Assuming that the intrinsic specific surface capacitances of both CZTS films are the same, the relative electrochemical area can be determined by the ratio of the capacitive current. Fig. 8(a) shows the capacitive currents of the dense CZTS photocathode with different scan rates of potentials. The relative area is calculated by comparing the capacitive currents under different scan rates and the results are shown in Fig. 8(b). The result shows that the porous CZTS film has about 4 times larger surface electrochemical area than the dense film. Since the dense and the porous samples have similar thickness (see Fig. 1c and d), the larger surface area of the porous sample suggests that more electrolyte can penetrate into the porous sample. Thus the average minority carrier transport distance from the bulk material to the semiconductor–electrolyte interface is shorter in the porous sample than that of the dense one. The effect of shorter carrier transport distance has also been observed in improving the performance of other porous materials.[25–28] Therefore, the shorter transport distance of minority carriers by the porous structure, not stronger light absorption, is the important reason for photocurrent enhancement. Even though, the carrier transport ability of the porous sample is still poor due to the nature of the nanocrystalline sample. A suitable method to increase the crystallinity of the porous sample is expected to be carried out to further improve the performance.

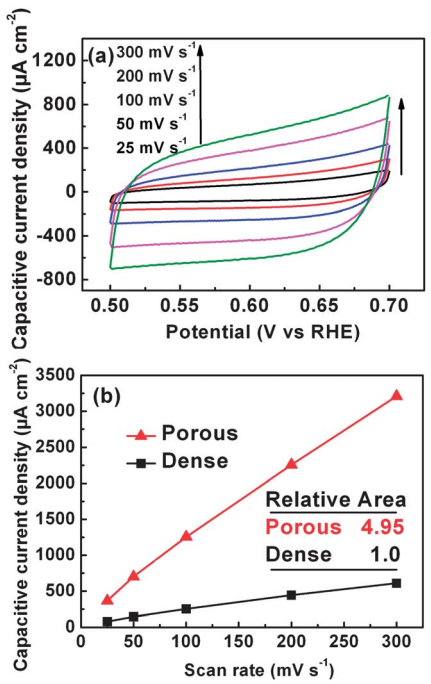

Fig. 8 (a) Cyclic voltammograms curves of the dense film at different scan rates of potentials from 25 to 300 mV s^{-1}. (b) The linear relationship between the capacitive current and the scan rate for both of the films, the relative electrochemically active surface areas are compiled in the inset table.

4. Conclusions

The dense and the porous nanocrystalline CZTS photocathodes have been successfully synthesized by tuning the thiourea/zinc ratios in the precursor solutions. The porous structure comes from the decomposition of excess amount of thiourea. The porous CZTS photocathode has 3 times higher photocurrent than that of the dense electrode. The shortening of the electron transport distance results in the improved photocurrent in the porous structure.

Acknowledgements

This work was supported by the National Basic Research Program of China (973 Program, 2013CB632404, 2014CB239303), the National Natural Science Foundation of China (no. 51272101), and the Jiangsu Provincial Natural Science Foundation (no. BK20130053).

References

1 A. Fujishima and K. Honda, *Nature*, 1972, **238**, 37.
2 M. G. Walter, E. L. Warren, J. R. McKone, S. W. Boettcher, Q. Mi, E. A. Santori and N. S. Lewis, *Chem. Rev.*, 2010, **110**, 6446.
3 Z. Li, W. Luo, M. Zhang, J. Feng and Z. Zou, *Energy Environ. Sci.*, 2013, **6**, 347.
4 C. Santato, M. Odziemkowski, M. Ulmann and J. Augustynski, *J. Am. Chem. Soc.*, 2001, **123**, 10639.
5 K. Sivula, F. Le Formal and M. Graetzel, *ChemSusChem*, 2011, **4**, 432.
6 W. Luo, Z. Yang, Z. Li, J. Zhang, J. Liu, Z. Zhao, Z. Wang, S. Yan, T. Yu and Z. Zou, *Energy Environ. Sci.*, 2011, **4**, 4046.
7 M. Li, W. Luo, D. Cao, X. Zhao, Z. Li, T. Yu and Z. Zou, *Angew. Chem., Int. Ed.*, 2013, **52**, 11016.

8 M. Liao, J. Feng, W. Luo, Z. Wang, J. Zhang, Z. Li, T. Yu and Z. Zou, *Adv. Funct. Mater.*, 2012, **22**, 3066.
9 D. Cao, W. Luo, M. Li, J. Feng, Z. Li and Z. Zou, *CrystEngComm*, 2013, **15**, 2386.
10 A. J. Nozik, *Appl. Phys. Lett.*, 1976, **29**, 150.
11 R. N. Dominey, N. S. Lewis, J. A. Bruce, D. C. Bookbinder and M. S. Wrighton, *J. Am. Chem. Soc.*, 1982, **104**, 467.
12 A. Heller and R. G. Vadimsky, *Phys. Rev. Lett.*, 1981, **46**, 1153.
13 Y. Z. Liu, J. L. Moll and W. E. Spicer, *Appl. Phys. Lett.*, 1970, **17**, 60.
14 D. Yokoyama, T. Minegishi, K. Maeda, M. Katayama, J. Kubota, A. Yamada, M. Konagai and K. Domen, *Electrochem. Commun.*, 2010, **12**, 851.
15 S. Huang, W. Luo and Z. Zou, *J. Phys. D: Appl. Phys.*, 2013, **46**, 235108.
16 H. Katagiri, K. Jimbo, W. S. Maw, K. Oishi, M. Yamazaki, H. Araki and A. Takeuchi, *Thin Solid Films*, 2009, **517**, 2455.
17 K. Wang, O. Gunawan, T. Todorov, B. Shin, S. J. Chey, N. A. Bojarczuk, D. Mitzi and S. Guha, *Appl. Phys. Lett.*, 2010, **97**, 143508.
18 B. Shin, O. Gunawan, Y. Zhu, N. A. Bojarczuk, S. J. Chey and S. Guha, *Prog. Photovoltaics Res. Appl.*, 2013, **21**, 72.
19 D. Yokoyama, T. Minegishi, K. Jimbo, T. Hisatomi, G. Ma, M. Katayama, J. Kubota, H. Katagiri and K. Domen, *Appl. Phys. Express*, 2010, **3**, 101202.
20 G. Ma, T. Minegishi, D. Yokoyama, J. Kubota and K. Domen, *Chem. Phys. Lett.*, 2011, **501**, 619.
21 L. Rovelli, S. D. Tilley and K. Sivula, *ACS Appl. Mater. Interfaces*, 2013, **5**, 8018.
22 A. Hagfeldt and M. Grätzel, *Acc. Chem. Res.*, 2000, **33**, 269.
23 H. Seel and R. Brendel, *Thin Solid Films*, 2004, **451–452**, 608.
24 G. Li, D. Zhang and J. C. Yu, *Chem. Mater.*, 2008, **20**, 3983.
25 B. M. Kayes, H. A. Atwater and N. S. Lewis, *J. Appl. Phys.*, 2005, **97**, 114302.
26 G. K. Mor, K. Shankar, M. Paulose, O. K. Varghese and C. A. Grimes, *Nano Lett.*, 2005, **5**, 191.
27 J. vande Lagemaat, M. Plakman, D. Vanmaekelbergh and J. J. Kelly, *Appl. Phys. Lett.*, 1996, **69**, 2246.
28 M. J. Price and S. Maldonado, *J. Phys. Chem. C*, 2009, **113**, 11988.
29 P. Dai, G. Zhang, Y. Chen, H. Jiang, Z. Feng, Z. Lin and J. Zhan, *Chem. Commun.*, 2012, **48**, 3006.
30 X. Yin, C. Tang, M. Chen, S. Adams, H. Wang and H. Gong, *J. Mater. Chem. A*, 2013, **1**, 7927.
31 B. A. Pinaud, P. C. K. Vesborg and T. F. Jaramillo, *J. Phys. Chem. C*, 2012, **116**, 15918.
32 J. Madarasz, P. Bombicz, M. Okuya and S. Kaneko, *Solid State Ionics*, 2001, **141**, 439.
33 Z. Y. Fan, H. Razavi, J. W. Do, A. Moriwaki, O. Ergen, Y. L. Chueh, P. W. Leu, J. C. Ho, T. Takahashi, L. A. Reichertz, S. Neale, K. Yu, M. Wu, J. W. Ager and A. Javey, *Nat. Mater.*, 2009, **8**, 648.
34 D. Kuang, J. Brillet, P. Chen, M. Takata, S. Uchida, H. Miura, K. Sumioka, S. M. Zakeeruddin and M. Gratzel, *ACS Nano*, 2008, **2**, 1113.
35 S. C. Riha, B. A. Parkinson and A. L. Prieto, *J. Am. Chem. Soc.*, 2009, **131**, 12054.
36 K. Sivula, R. Zboril, F. Le Formal, R. Robert, A. Weidenkaff, J. Tucek, J. Frydrych and M. Gratzel, *J. Am. Chem. Soc.*, 2010, **132**, 7436.
37 C. Santato, M. Ulmann and J. Augustynski, *Adv. Mater.*, 2001, **13**, 511.
38 P. A. Fernandes, P. M. P. Salomé and A. F. da Cunha, *Thin Solid Films*, 2009, **517**, 2519.
39 X. Fontane, L. Calvo-Barrio, V. Izquierdo-Roca, E. Saucedo, A. Perez-Rodriguez, J. R. Morante, D. M. Berg, P. J. Dale and S. Siebentritt, *Appl. Phys. Lett.*, 2011, **98**, 181905.
40 M. G. Sousa, A. F. da Cunha, P. M. P. Salomé, P. A. Fernandes, J. P. Teixeira and J. P. Leitão, *Thin Solid Films*, 2013, **535**, 27.
41 S. Chen, X. G. Gong, A. Walsh and S.-H. Wei, *Appl. Phys. Lett.*, 2010, **96**, 021902.
42 S. Chen, J.-H. Yang, X. G. Gong, A. Walsh and S.-H. Wei, *Phys. Rev. B: Condens. Matter Mater. Phys.*, 2010, **81**, 245204.